



HAL
open science

Experimental validation of the strut-and-tie design for reinforced concrete massive structures by deformation flow analysis

Mihaja Razafimbelo, Fabrice Gatuingt, Guillaume Hervé-Secourgeon, Marina Bottoni, Xavier Pinelli, Túlio Honório, Magdalini Titirla

► To cite this version:

Mihaja Razafimbelo, Fabrice Gatuingt, Guillaume Hervé-Secourgeon, Marina Bottoni, Xavier Pinelli, et al.. Experimental validation of the strut-and-tie design for reinforced concrete massive structures by deformation flow analysis. fib International Congress 2022, Jun 2022, Oslo, Norway. hal-03699690

HAL Id: hal-03699690

<https://hal.science/hal-03699690v1>

Submitted on 20 Jun 2022

HAL is a multi-disciplinary open access archive for the deposit and dissemination of scientific research documents, whether they are published or not. The documents may come from teaching and research institutions in France or abroad, or from public or private research centers.

L'archive ouverte pluridisciplinaire **HAL**, est destinée au dépôt et à la diffusion de documents scientifiques de niveau recherche, publiés ou non, émanant des établissements d'enseignement et de recherche français ou étrangers, des laboratoires publics ou privés.

EXPERIMENTAL VALIDATION OF THE STRUT-AND-TIE DESIGN FOR REINFORCED CONCRETE MASSIVE STRUCTURES BY DEFORMATION FLOW ANALYSIS

Mihaja Razafimbelo^{1,2}, Fabrice Gatuingt¹, Guillaume Hervé-Secourgeon^{1,2}, Marina Bottoni²,
Xavier Pinelli¹, Túlio Honório¹, Magdalini Titirla³

¹ Université Paris-Saclay, CentraleSupélec, ENS Paris-Saclay, CNRS, LMPS - Laboratoire de Mécanique Paris-Saclay, 91190, Gif-sur-Yvette, France

² Institute of Mechanical Sciences and Industrial Applications, EDF-CNRS-CEA-ENSTA UMR 9219, and EDF, R&D Department, Palaiseau, France

³ LMSSC Laboratoire de Mécanique des Structures et des Systèmes Couplés, Le Cnam, Paris

* Corresponding author : Mihaja Razafimbelo (mihaja.razafimbelo@ens-paris-saclay.fr)

ABSTRACT

The design of reinforced concrete structures follows prescriptions of codes and standards (e.g., ACI and Eurocode). The strut-and-tie method is the only approach detailed in standards for the design of reinforcement of massive structures. Strut-and-tie methods are currently showing a strong interest and several techniques are based on automatic strategies and topological optimization. However, this method is based on a strong hypothesis associated with linear elastic analyses. In particular, the occurrence of pre-existing cracks is not considered when drawing the strut-and-tie model. This work aims to understand the role of an initially cracked state and, thus, the loading history in the design and choice of strut and tie directions. An experimental test is analyzed for a real size corbel loaded in two different in-plane directions with forces not applied simultaneously. Hence, the specimen was cracked when the second force was applied.

The corbel has minimal reinforcement to avoid brittle failure but should not affect the crack directions. The instrumentation used, combining digital image correlation and optical fiber sensing, allows for monitoring during the test and provides insight into the cracking history and the deformations in visible surfaces and in the bulk. Digital image correlation was used over the entire top surface of the corbel to measure displacement fields and thus strain fields, as well as information on cracking during the test. Optical fibers were installed within the specimen to measure strains in bulk. This measurement allows for the detection of cracks in the sample volume and thus complements digital image correlation measurements for fibers close to the surface. The results provide key data on the flow history of mechanical fields within the structure under different loads. This information helped clarify the domain of validity of strut-and-tie fundamental assumptions and may improve this design approach.

Keywords: strut and tie, experimental test, concrete, validation

1. INTRODUCTION

The strut-and-tie method (STM) is proposed by the standards (e.g. Eurocode [1], ACI [2] or FIB [3]) to design the steel reinforcement in massive or discontinuity regions in concrete structures. Historically, it was derived from the so-called Ritter-Mörsch method [4] - [5] for beams subjected to shear, based on the determination of a truss equivalent to the initial structure in supporting external forces. This main principle was further developed by Schlaich [6] and generalized to discontinuity and massive zones.

Like most traditional design methods to reinforce concrete, strut-and-tie design is conducted based on the hypothesis (1) forces and stresses are obtained from linear elastic calculations, and (2) that such calculations are performed on unreinforced structures. This paper addresses the first of the two previous hypotheses, particularly one of its corollaries, namely, that the loading history has no effect on the

current distribution of stresses and on steel reinforcements. This statement is debatable because design in concrete structures always implies cracking (here necessary to the appropriate identification of struts).

In order to discuss linearity in design, experimental tests were performed on a corbel instrumented with optical fibers for real-time assessment of mechanical fields. The corbel was submitted to two forces applied one after the other. For both loads, they were applied until cracking of the specimen to go beyond the elastic phase. The test had two different aims. First, it was carried out to understand how cracking affects strut distributions on the corbel. Second, it is to provide a set of experimental validation data concerning the strain path and crack pattern with the same level of details as in FE results. The test presented herein has to be considered within a series of 3 sub-tests involving different combinations of forces in order to challenge the appropriateness of superposition hypotheses in the cracking history for the optimization of STMs. The specimen was monitored by both optical fibers and digital image correlation (DIC), allowing for continuous measurement of displacement and strain fields.

2. EXPERIMENTAL SET-UP

2.1. Description of the specimen

The corbel geometry and reinforcement details are defined in Figure 1. The reference frame for the strut-and-tie method was homogeneous, elastic and sound (i.e., unreinforced) concrete. A minimal reinforcement was added to maintain the structure during test preparation and force application. The reinforcement was also helpful as a support to the optical fibers. Anchoring rods and plates were inserted for gripping and force application.

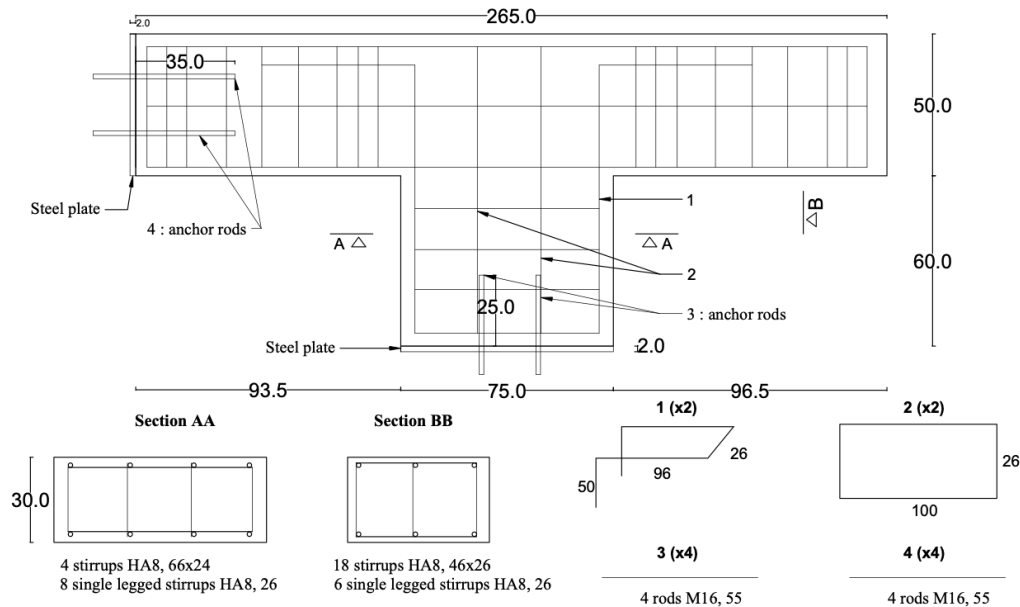


Figure 1: Steel reinforcement of the specimen (unit: cm and mm for rebars)

2.2. Material properties

An ordinary concrete of class C30/37 (Eurocodes notation) was used. Compression and splitting tests performed 28 days after concrete casting provided the mechanical properties of concrete. The value of Young modulus, compressive and tensile strength are respectively $E_c = 36.11$ GPa and $f_c = 35.40$ MPa (which are the average values over 9 compression specimens and a standard deviation of 0.596 GPa for Young's Modulus and 1.73 MPa for compressive strength) and tensile strength $f_t = 3.1$ MPa (9-sample average with 0.24 MPa as standard deviation). These results correspond to high values for concrete of the chosen class. The test on the corbel was performed 30 days after concrete casting.

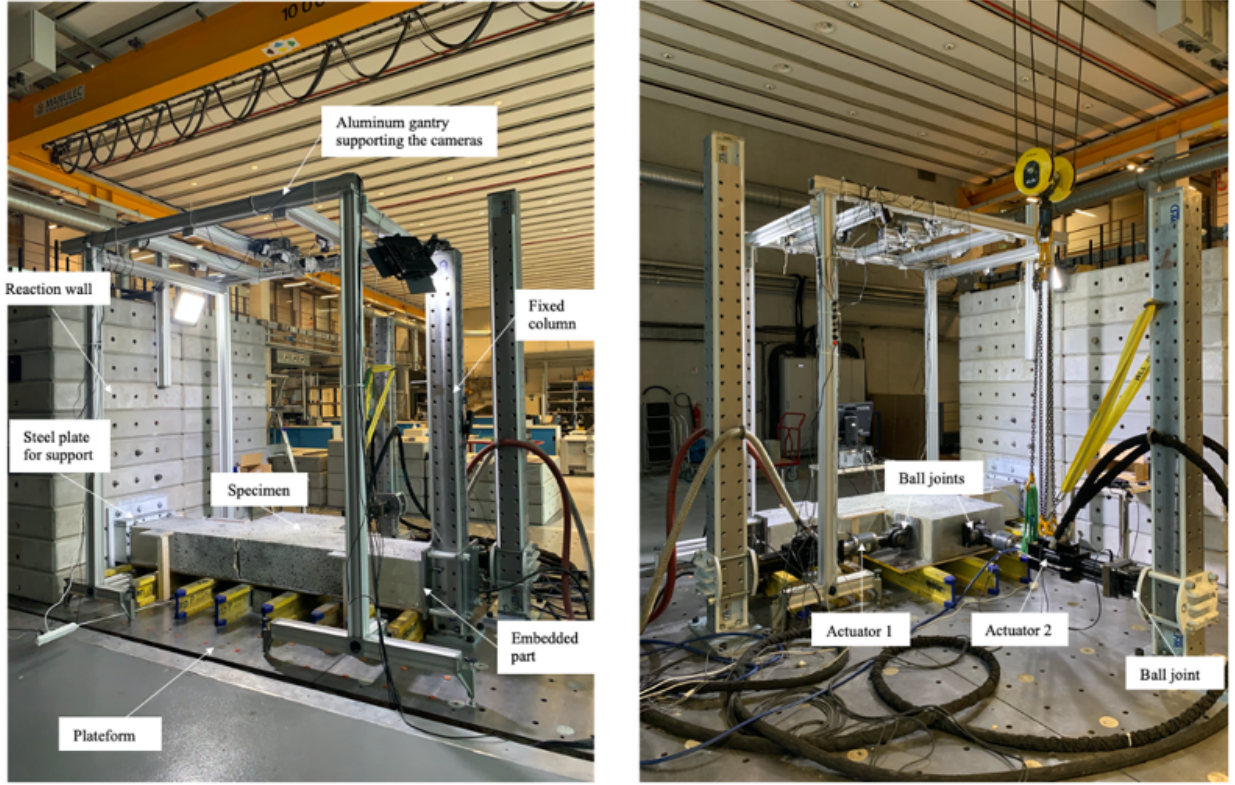


Figure 3: Photos of the experimental set-up.

2.4.1. Digital image correlation

Digital image correlation is an experimental technique to measure a displacement field by matching digital pictures of an object before and during deformation [7]. All algorithms start with what is called the "conservation of brightness". The concept is that a material point will have the same gray level and intensity in each image, regardless of its position in the image. In the absence of acquisition noise, there should be no difference between the gray level of a material point P denoted by the vector \underline{x} in the reference image f , and that of the same material point in a second image g where the point is assumed to have moved with a displacement $\underline{u}(\underline{x})$. Mathematically, this is expressed as follows:

$$f(\underline{x}) = g(\underline{x} + \underline{u}(\underline{x})) \quad (1)$$

Considering brightness conservation for all material points in the region of interest (ROI), a least squares cost function reads:

$$\Theta = \sum_{ROI} \left(f(\underline{x}) - g(\underline{x} + \underline{u}(\underline{x})) \right)^2 \quad (2)$$

The only unknowns are the parameters of the displacement field that minimize the previous cost function.

To have confidence in the measurements, calibration targets (CC) were fixed to the platform, uncoupled from the specimen, and seen by the cameras. Kept in place, these calibration targets allow small drifts to be corrected. For this, an error coefficient which corresponds to a standard deviation of the displacements of the calibration test patterns is calculated on a zone of interest which is the test pattern and another zone on the specimen. The difference of this error highlights the recalibration of displacement, which is necessary to obtain a correct displacement.

The correlation of images allows obtaining a displacement field and then deriving a deformation field. We use the cameras independently of the others first to locate the cracks for this study. We want to identify the cracks during the first loading before breakage then the cracks after the second loading by maintaining the first.

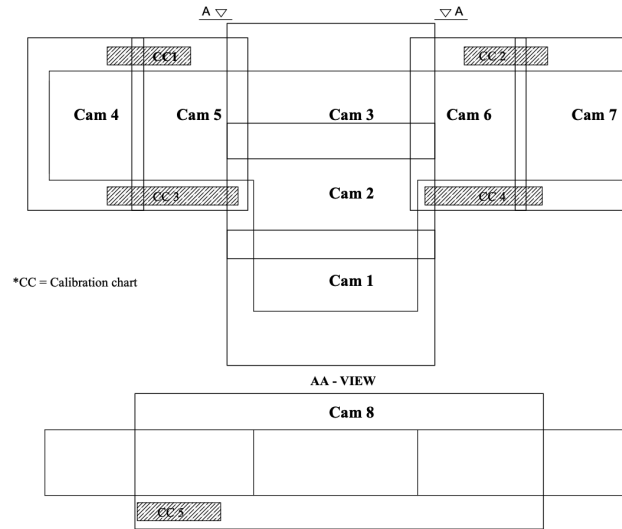


Figure 4: Position of cameras and overlap areas

2.4.2. Optical fiber measurements

Optical fibers are currently used for structure health monitoring because of multiple advantages such as the possibility of continuous measurements, their small size, and the fact that they are passive sensors. Fibers that use Rayleigh diffusion were selected. This Rayleigh diffusion uses the heterogeneities of index profile along the fiber. A laser pulse is sent and propagates in the fiber for this type of sensors based on Rayleigh scattering. Because of heterogeneities of silica, a part of the light is backscattered at each point. The power of this backscattered light is detected at the end of the fiber connected to a reflectometer. Thanks to time of flight evaluations, the location of the events is traced along the fiber. The time between the emission of the pump laser and the reception of the reflected signal allows the position of the scattering element to be located. When Rayleigh backscatter is measured in an undisturbed state and over a certain spectral range, and the response of this signature is correlated in a disturbed state (by temperature, strain or other), a spectral offset is detected. This Rayleigh spectral offset $\Delta\nu^R$ depends on both temperature ΔT and strain ε (relative elongations)

$$\Delta\nu^R = C\varepsilon^R \cdot \varepsilon + CT^R \cdot \Delta T \quad (3)$$

where $C\varepsilon^R$ et CT^R are the calibration coefficients for strain and relative temperature measurements, respectively. In the present case, the values of the calibration coefficients were $C\varepsilon^R = -0.15 \text{ GHz}/\mu\varepsilon$ and $CT^R = -1.25 \text{ GHz}/^\circ\text{C}$. The mechanical strains are obtained with the Rayleigh spectral shift affected by the calibration coefficient with the necessary condition of thermal stabilization in concrete. The fibers were placed in concrete along the reinforcement following Figure 5.

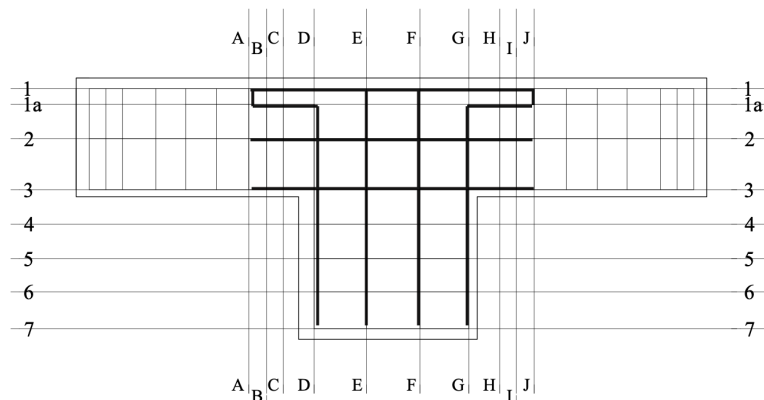


Figure 5: Optical fibers frame in the specimen

3. RESULTS

3.1. Global loading curves

Figure 6 show the force-displacements for the two jacks, with displacements measured on the jacks itself. These graphs provide us with some useful information and allow us to identify some characteristic times on the curves. For the first actuator (orange curve), time T0 is the beginning of the first jack load. T1 time instant (924 s) corresponds to a decrease of the applied force. This drop marks the end of the elastic phase and may be due to a first crack opening. Time T2 (1260 s) marks a large load drop (from 80 kN to 30 kN). However, after this drop, the tangent stiffness of the loading curve remained close to that in the elastic phase. T3 (2269 s) marks another load drop and a strong change in slope, it is shown in post-processing that a crack appears and it is viewed by monitoring (with fiber optic peaks §3.3 and digital image correlation §3.4). At 120 kN (T-F1), the first hydraulic jack was maintained at constant force (see Figure 2).

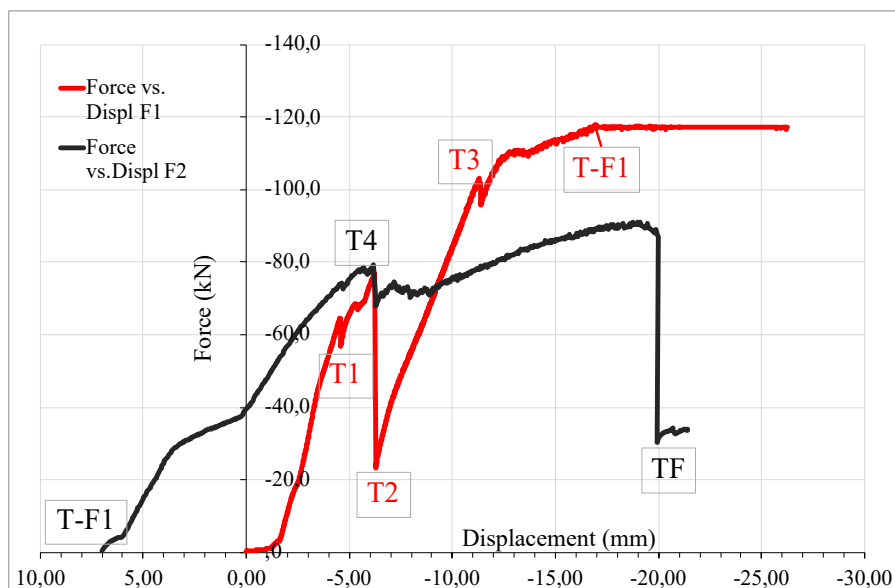


Figure 6: Force vs. displacement graph for the first and second actuator

The motion of the first jack created a motion of the second jack because the ball joint allowed this to occur (see Figure 6). As a consequence, T-F1 is taken as the reference level of the second jack displacement (black curve). Changes in stiffness are observed without large drops. At time T4 (3669 s), a loss of 10 kN is observed, which marks crack inception and propagation of a second main crack in the specimen (see later in §3.1). At the end of the test (time FT), the opening of this same crack occurred causing a strong loss of stiffness of the specimen.

3.2. Digital Image Correlation results

Thanks to DIC, the actual force vs. displacement graph (Figure 6) was obtained by post-processing displacements at the load application areas. In fact, displacements recorded by the jack and those measured on the load application point are different, the first being more or less double then the second. From a qualitative point of view, we find the same characteristic time instants than in Figure 7, when the opening of cracks provoke drops in the applied force.

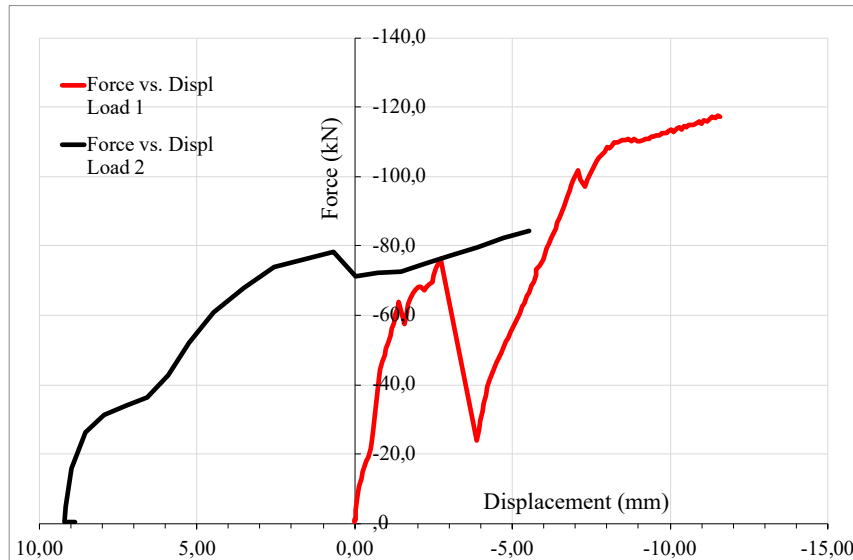


Figure 7: Force vs. Displacement graph using image correlation (Load 1 and Load 2)

The results shown hereafter (Figure 8 and Figure 9) correspond to maximum and minimum eigenstrain fields derived from the displacements measured for cameras 2 and 3. Depending on the loading, the principal direction of strain vary significantly. With the second loading, a bottle-shaped connecting strut is clearly highlighted. Results also show the forming of cracks and their evolution during the test.

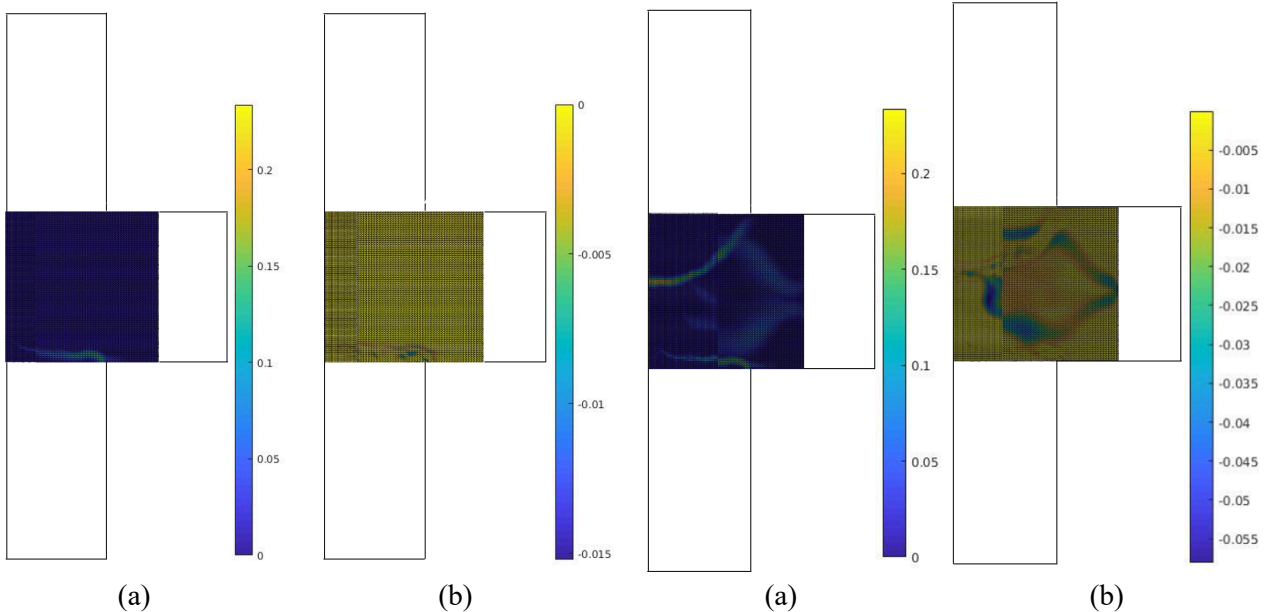


Figure 8: maximum eigen strain after F1 charging (a) extension ; (b) contraction

Figure 9: maximum eigen strain at the end of the test (F1+F2) (a) extension ; (b) contraction

It shows the cracks and their evolution during the test. Eventually, the advantage of the correlation is that it is possible to superimpose the result on a mesh and to use post-processing as validation

3.3. Optical fiber readings

Figure 10 shows the strain profile along the line D7-D1a for three specific time instants, T1, T2, T3 (defined in §3.1), T1, T2 and T3: T1 and T2 show indeed an increase in tension between the points D3 and D2; this peak breaks in two subpeaks at time T3, marking the apparent opening of a secondary crack. In Figure 11, the evolution of strain between line 2 and 3 on the D frame, we call it D23, is represented.

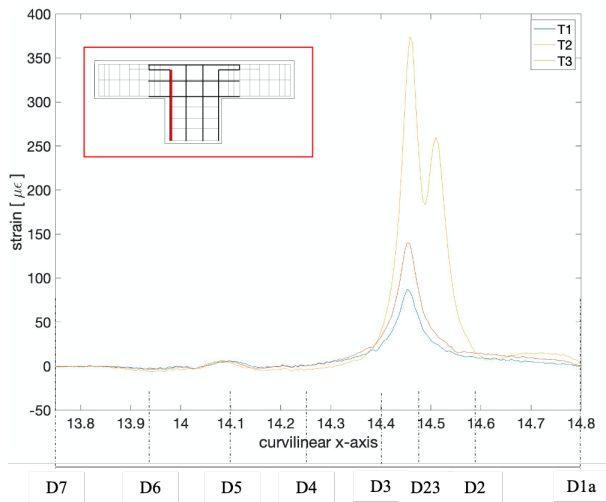


Figure 10: Evolution of strain along curvilinear abscissa D7D1

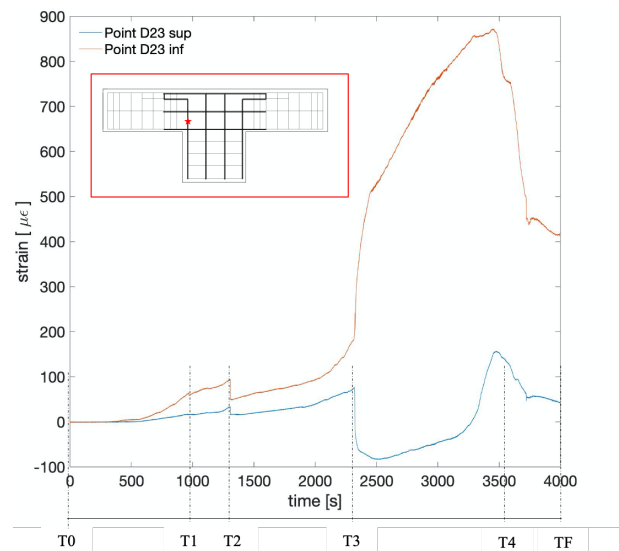


Figure 11: Temporal evolution of strain in the D23 point measured in the superior fiber and inferior one

We observe the evolution of the extension for both lower and upper points until T3 (Figure 11). The level of deformation is more important in the lower part and we have a crack from time T2. As for the upper part, the crack opens from T3. At this time, the extension continued in the lower part. But we have a contraction in the upper part: this effect can be explained by the effect of the second loading which brings compression and whose effect is more repercussive at the top of the specimen.

At time T4, cracks are detected near points G1, F1 and D1 located inside the concrete (Figure 12 Figure 13). at the point D1, we watch an increasing extension starting from T3, that is during the whole loading of F2. The other points (G1 and F1) show peaks at the end, after T4, which is manifested by the cracks .

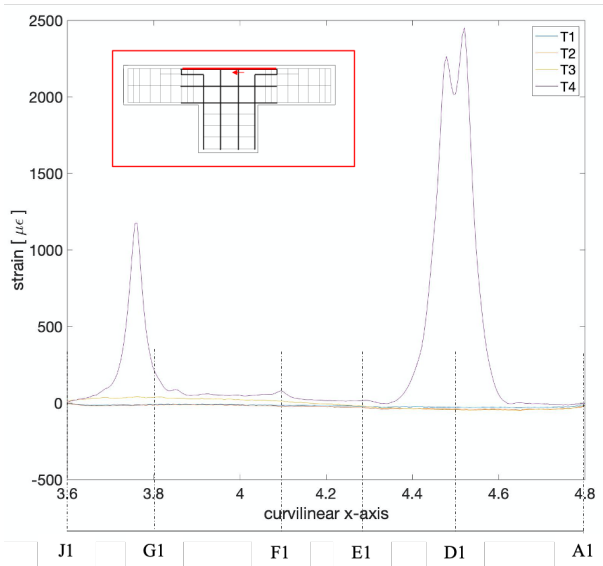


Figure 12: Strain profile of the line J1A1 with peaks of strain at G1, F1 and D1

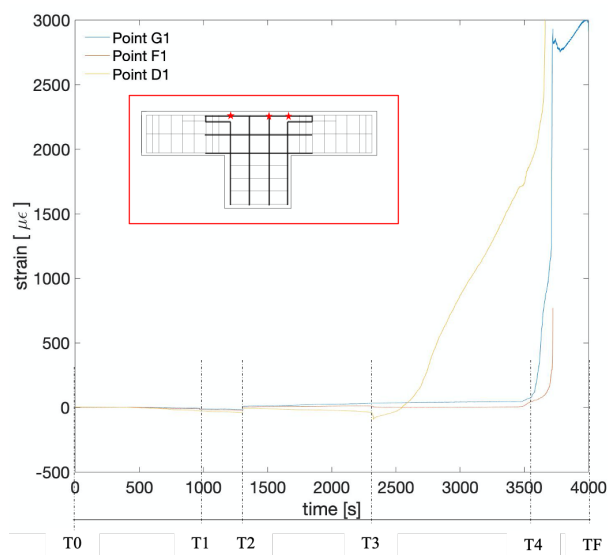


Figure 13: Temporal evolution of strain in the point G1, F1 and D1

It is observed that the measurements are consistent with what the DIC results show, including crack initiation.

3.4. Post-mortem analysis of the specimen

The post-mortem analysis of the specimen starts with the observation of the main cracks.

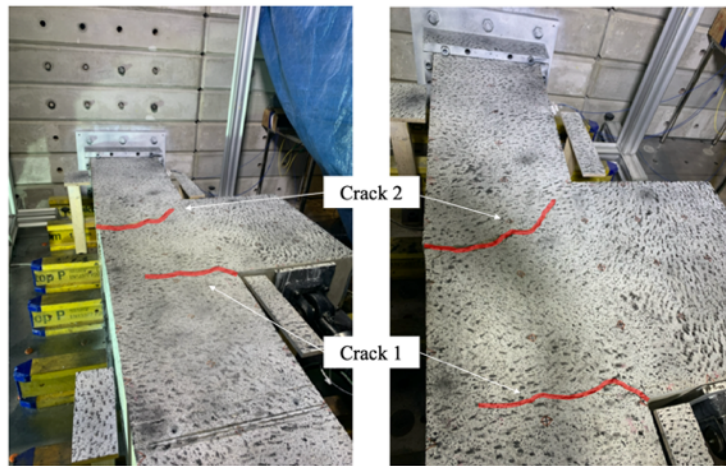


Figure 14: Two main cracks on the specimen surface

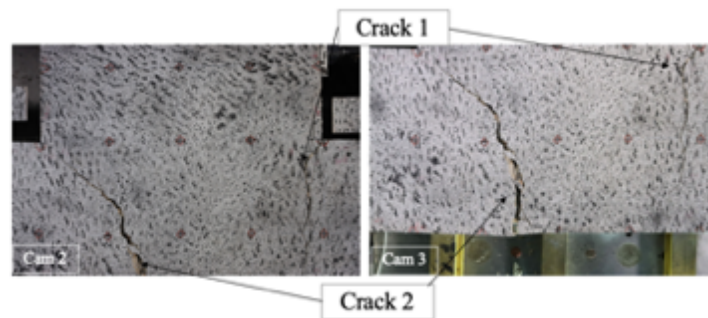


Figure 15: Cracks view on the top

They are well identifiable with bare eyes but some seem more difficult to see. In particular, at the level of the spline, two additional cracks are detected thanks to the measured strains by optical fiber and also via DIC.

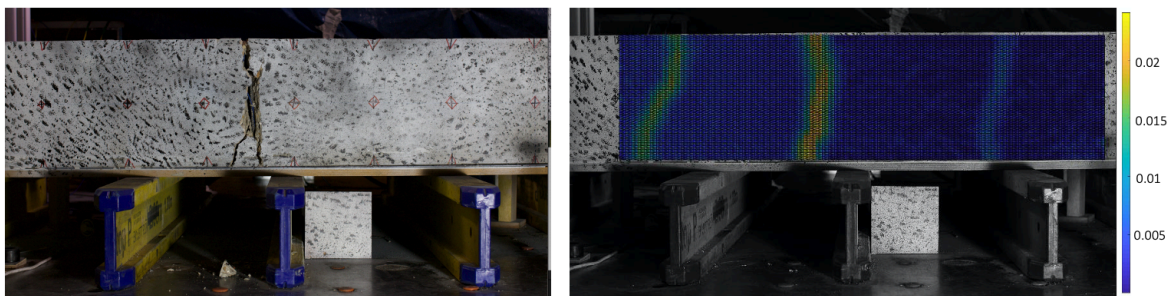


Figure 16: Crack on the spline and maximum eigen strain measured via DIC

The test stopped when the force applied by the second jack decreased. The maximum force level of the latter was about 90 KN. During the test, the development of cracking follows the isostatic extension line and justifies the consideration of the linear elastic behavior to define the model. The understanding of the behavior of concrete allows the first cracks to be detected still invisible on the surface. The strain fields determined by DIC will enable a global vision of the entire specimen and serve as a basis for further design.

4. CONCLUSIONS AND PERSPECTIVES

The whole work consisted of performing a complex test on concrete. It had for interest to study the behavior of as massive structures where rebars design is usually done by the strut-and-tie method. The

instrumentation chosen allowed for real-time monitoring of the deformation of the studied structure (internal with optical fibers and external via DIC). The optical fibers gave information about internal strains in the structure and the inception of the first cracks. DIC also provided a global view of the specimen with the temporal evolution of displacement and strain fields. The first DIC results make it possible to obtain eigenstrain fields derived from the displacement fields. This test corresponds then to a reliable basis of experimental validation of struts-and-tie methods.

The aim of the described test is to understand how the damaged state at the end of loading F1 affects the struts distribution and then the design of steel reinforcement by the strut-and-tie method. To do so, displacements and strains issued from DIC post-processing will be first compared with numerical simulations, in the linear and non-linear domain. Moreover, a second experimental test will be performed, where forces F1 and F2 are applied simultaneously to the corbel.

5. REFERENCES

- [1] N. EN1992-1-1, Eurocode 2 - Calcul des structures en béton - Partie 1-1: règles générales et règles pour les bâtiments - Section 6 : Dimensionnement à l'aide de modèles bielles-tirants.
- [2] A. PRC-445, 2-21: Strut-and-Tie Method Guidelines for ACI 318-19 - Guide.
- [3] I. F. f. S. C. (fib), Model code - Bulletin N65, 2012.
- [4] W. Ritter, Die Bauweise Hennebique, vol. V33 vcl, Zürich: Schweizerische Bauzeitung, 1899, pp. 59-61.
- [5] E. Mörsch, Der Eisenbetonbau, seine Anwendung und Theorie, New York: Me Graw-Hill, 1902.
- [6] J. Schlaich, Toward a consistent design of structural concrete, PCI Journal, 1987.
- [7] F. Hild and S. Roux, "Comparison of local and global approaches to digital image correlation," *Experimental mechanics*, 2012.
- [8] J.-L. Bosc, Dimensionnement des constructions selon l'Eurocode 2 à l'aide des modèles Bielles et Tirants, Presses de l'école nationale des Ponts et chaussées.
- [9] G. M. Chavez, Approche semi-automatique de génération de modèles bielles-et-tirants, 2015.
- [10] Q. Q. Liang, "Topology Optimization of Strut-and-Tie Models in Reinforced Concrete Structures Using an Evolutionary Procedure," *Aci Structural Journal*, vol. 97(2), pp. 322-332, 2000.